

Boosting the Deep Discharging/Charging Lithium Storage Performances of Li_3VO_4 through Double-Carbon Decoration

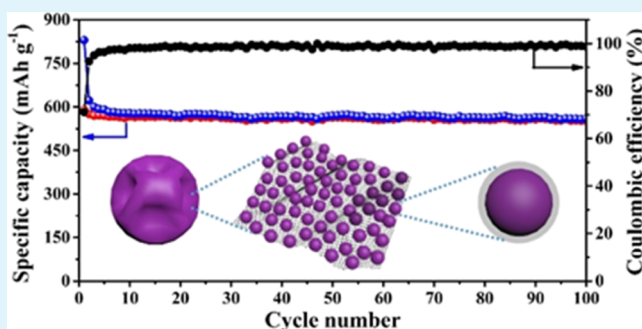
Huancheng Liu, Ping Hu, Qiang Yu, Zhenhui Liu, Ting Zhu, Wen Luo, Liang Zhou,*^{1b} and Liqiang Mai*^{1b}

State Key Laboratory of Advanced Technology for Materials Synthesis and Processing, Wuhan University of Technology, Wuhan 430070, P. R. China

Supporting Information

ABSTRACT: With high theoretical capacity, good ionic conductivity, and suitable working plateaus, Li_3VO_4 has emerged as an eye-catching intercalation anode material for lithium storage. However, Li_3VO_4 suffers from poor electrical conductivity and 20% volume variation under deep discharging/charging conditions. Herein, we present a “double-carbon decoration” strategy to tackle both issues. Deflated balloon-like $\text{Li}_3\text{VO}_4/\text{C}/\text{reduced graphene oxide}$ (LVO/C/rGO) microspheres with continuous electron transport pathways and sufficient free space for volume change accommodation are fabricated through a facile spray-drying method. Under deep discharging/charging conditions (0.02–3.0 V), LVO/C/rGO achieves a high intercalation capacity of 591 mA h g^{-1} . With high capacity and outstanding stability, LVO/C/rGO outperforms other intercalation anode materials (such as graphite, $\text{Li}_4\text{Ti}_5\text{O}_{12}$, and TiO_2). In situ X-ray diffraction measurement reveals that the lithium storage is realized through both solid-solution reaction and two-phase reaction mechanisms. A LVO/C/rGO// $\text{LiNi}_{0.8}\text{Co}_{0.15}\text{Al}_{0.05}\text{O}_2$ lithium-ion full cell is also assembled. In such full cell, LVO/C/rGO also demonstrates high specific capacity and excellent cycling stability. The above results manifest that the LVO/C/rGO anode has the potential to be applied in the next-generation high-performance lithium-ion batteries.

KEYWORDS: Li_3VO_4 , spray drying, intercalation anode, lithium-ion battery, double-carbon decoration



1. INTRODUCTION

Lithium-ion batteries (LIBs) with higher energy density, better safety, and lower cost are urgently required because of the fast-growing market demand of grid-scale energy storage, portable electronics, and electric vehicles.^{1–5} Nowadays, most of the commercial LIBs employ intercalation anode materials, such as graphite and $\text{Li}_4\text{Ti}_5\text{O}_{12}$. However, both graphite and $\text{Li}_4\text{Ti}_5\text{O}_{12}$ share the common feature of limited theoretical capacity, making them difficult to meet the ever-increasing requirements. In addition, graphite has a low Li^+ insertion potential ($\sim 0.1 \text{ V}$ vs Li^+/Li) close to Li plating, which may cause serious safety issues. $\text{Li}_4\text{Ti}_5\text{O}_{12}$ has safer Li^+ insertion potential (1.5 V vs Li^+/Li) and zero volume change, but the theoretical value of gravimetric capacity for $\text{Li}_4\text{Ti}_5\text{O}_{12}$ is merely 175 mA h g^{-1} .^{6,7} Therefore, it is essential to develop alternative anode materials with higher theoretical capacity and more suitable Li^+ insertion potential.

Li_3VO_4 has long been known as an ionic conductor.⁸ In 2013, Li et al. first proposed the application of Li_3VO_4 as an anode material for LIBs.⁹ When compared to commercial graphite and $\text{Li}_4\text{Ti}_5\text{O}_{12}$, the Li_3VO_4 possesses more suitable Li^+ insertion potential (0.5–1.0 V) and higher theoretical capacity.¹⁰ Under shallow discharging/charging conditions, two Li ions can be accommodated by per formula of Li_3VO_4 ,

leading to a limited theoretical capacity of 394 mA h g^{-1} . Under deep discharging/charging conditions, three Li ions can be accommodated, resulting in an increased theoretical capacity of 592 mA h g^{-1} .^{11–13} Such a remarkable intercalation capacity would lead to significant improvement in energy density when coupled with appropriate cathode materials.¹⁴ However, the high specific capacity realized through deep discharging is accompanied by a relatively large volume expansion ($\sim 20\%$).¹³

Despite the multiple merits (high capacity, good ionic conductivity,¹⁵ and suitable Li^+ insertion potential), the commercial application of Li_3VO_4 in LIBs has been restricted by its poor electronic conductivity ($< 10^{-10} \text{ S m}^{-1}$).^{16–18} To improve the electronic conductivity, significant efforts have been dedicated to compositing Li_3VO_4 with various carbon materials, such as amorphous carbon/partially graphitized carbon,^{19–28} graphene/graphene oxide (GO),^{16,29–32} natural graphite,³³ and carbon nanotubes.^{34,35} Coupling with Ni foam,³⁶ introducing oxygen vacancies,³⁷ and M-doping (M = Ni, Mo, Ca, Cu, and Ti)^{38–42} have also been demonstrated to

Received: May 22, 2018

Accepted: June 26, 2018

Published: June 26, 2018

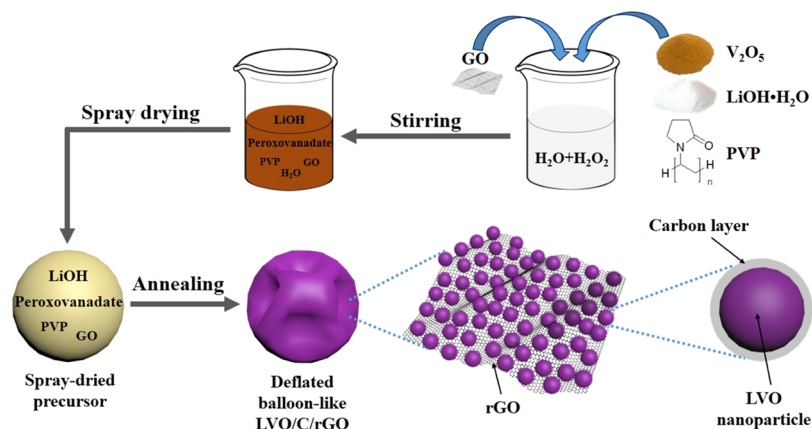


Figure 1. Schematic illustration of the synthesis process of the deflated balloon-like LVO/C/rGO microspheres.

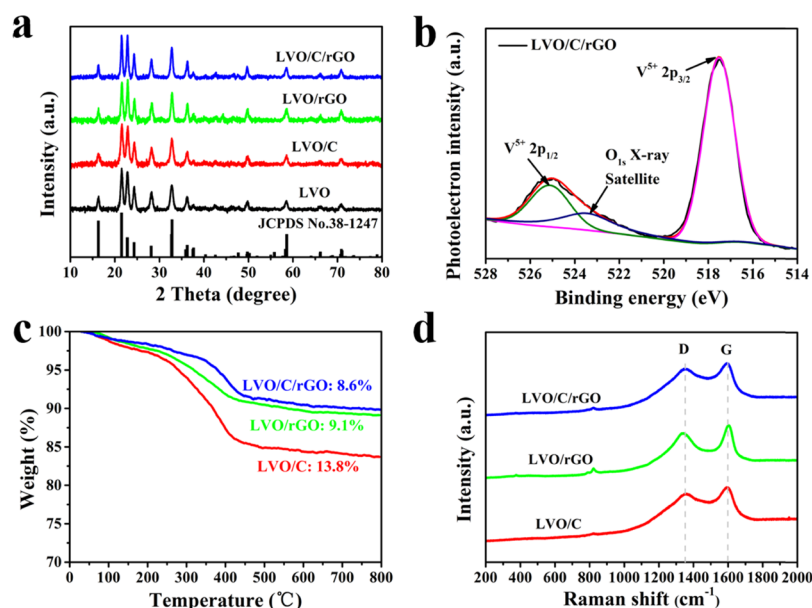


Figure 2. (a) XRD patterns of LVO, LVO/C, LVO/rGO, and LVO/C/rGO; (b) V 2p XPS spectrum of LVO/C/rGO; (c) TGA curves and (d) Raman spectra of LVO/C, LVO/rGO, and LVO/C/rGO.

be effective in enhancing the electronic conductivity. In addition, fabricating delicate nanostructures can also be employed to reduce the electron/ion transport path and thus boost the electrochemical performances.^{43,44} However, most previous studies evaluated the lithium storage performances and mechanisms of Li_3VO_4 under shallow discharging/charging conditions (0.2–3.0 V), which restricted the energy density of full cells.

Herein, we present a “double-carbon decoration” strategy to tackle the electrical conductivity and volume change issues of Li_3VO_4 . Deflated balloon-like LVO/C/rGO microspheres are produced by a scalable and continuous spray-drying process. The major active component, Li_3VO_4 , provides efficient lithium-ion diffusion channels and high intercalation capacity. Meanwhile, the double-carbon matrix (rGO and amorphous carbon) greatly enhances the electrical conductivity and accommodates the volume variation of Li_3VO_4 nanoparticles. Therefore, the obtained LVO/C/rGO demonstrated high specific capacity (591 mA h g^{-1} at 100 mA g^{-1}) and outstanding cyclability (350 mA h g^{-1} after 1000 cycles at 2000 mA g^{-1}) in lithium storage under deep discharging/charging condition, namely, 0.02–3.0 V. The excellent

electrochemical performances suggest that the LVO/C/rGO nanocomposite would be a potential anode material for high-energy-density LIBs.

2. EXPERIMENTAL SECTION

GO was synthesized through the well-known Hummers method.⁴⁵ The LVO/C/rGO microspheres were prepared through a scalable spray-drying method. First, 10 mL of H_2O_2 (30 wt %), 0.91 g of V_2O_5 , 1.275 g of $\text{LiOH}\cdot\text{H}_2\text{O}$, 0.25 g of poly(vinylpyrrolidone) (PVP, K-30), and 7.5 mL of GO (8.7 mg mL^{-1}) were added into 100 mL of H_2O with ultrasonic dispersion and stirring at room temperature until getting a homogeneous suspension. The obtained suspension was spray-dried using a BUCHI Mini Spray Dryer B-290. The detailed parameters about spray-drying process were listed as follows: aspirator rate: 90%, pump rate: 5%, inlet temperature: $220 \text{ }^\circ\text{C}$, and rotameter setting: 40 mm. Finally, the LVO/C/rGO composite was obtained by annealing the obtained dry powder at $500 \text{ }^\circ\text{C}$ for 5 h in N_2 . For comparison, LVO/rGO, LVO/C, and LVO were also synthesized via similar procedures except that no PVP was used for the fabrication of LVO/rGO, no GO was used for the fabrication of LVO/C, neither PVP nor GO was used for the fabrication of LVO.

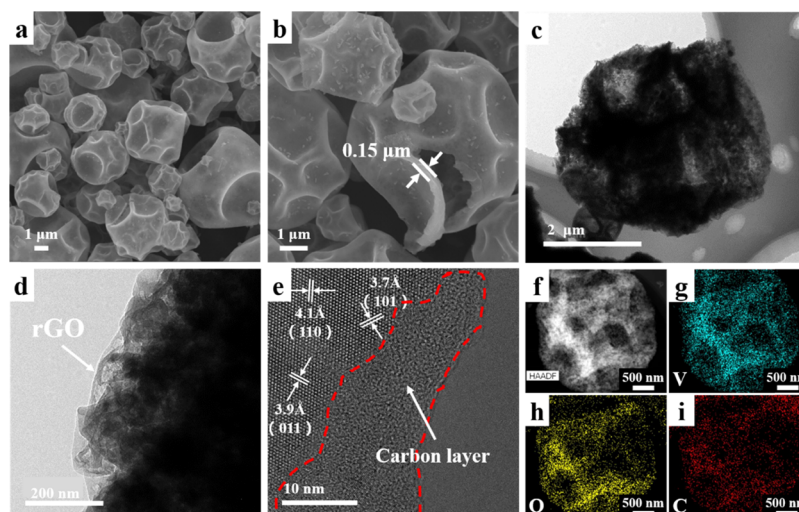


Figure 3. (a,b) SEM images of LVO/C/rGO; (c,d) TEM images of LVO/C/rGO; (e) HRTEM image of LVO/C/rGO; (f) HAADF image of an individual LVO/C/rGO microsphere; and (g–i) EDS mappings of V, O, and C elements in the single LVO/C/rGO microsphere.

3. RESULTS AND DISCUSSION

The LVO/C/rGO microspheres were produced through a scalable spray-drying process with subsequent annealing (Figure 1). First, the dispersion containing peroxovanadate, LiOH, PVP, and GO was quickly sprayed into microdroplets with a two-fluid nozzle atomizer under airflow. The water in the microdroplets was then quickly evaporated in the drying chamber at high temperatures (150–220 °C). The deflated balloon-like LVO/C/rGO microspheres were obtained after annealing in N₂. In the constructed architecture, the rGO forms a three-dimensional, continuous, and flexible electronic conductive network. The PVP-derived amorphous carbon matrix hosts the crystallized LVO nanoparticles and firmly anchors the LVO nanoparticles on rGO.

X-ray diffraction (XRD) is applied to analyze the crystalline phase of the obtained products (Figure 2a). All diffractions of the samples are assigned to β -Li₃VO₄ (JCPDS no. 38-1247). No impurity peak is detected, demonstrating the high purity of the samples. From the XRD pattern, the average crystallite size of Li₃VO₄ in the LVO/C/rGO composite is calculated to be 26.9 nm using Scherrer equation. X-ray photoelectron spectroscopy (XPS) is measured to detect the valence states of V for LVO/C/rGO (Figure 2b). Two dominant peaks are observed at 517.52 and 525.12 eV, matching with the 2p_{3/2} and 2p_{1/2} spin-orbit levels of V⁵⁺, respectively. The carbon contents of the samples are determined by thermogravimetric analysis (TGA). From the TGA curves, the carbon contents of LVO/C, LVO/rGO, and LVO/C/rGO composites are determined to be approximately 13.8, 9.1, and 8.6 wt %, respectively (Figure 2c). The Raman spectra (Figure 2d) of LVO/C, LVO/rGO, and LVO/C/rGO show two evident broadened peaks at 1350 cm⁻¹ (namely, D-band of carbon) and 1594 cm⁻¹ (namely, G-band of carbon). The graphitization degree of carbonaceous materials can be generally reflected from the I_D/I_G ratio. LVO/C, LVO/rGO, and LVO/C/rGO exhibit similar I_D/I_G ratio, indicating that the difference in graphitization degree is negligible in these products. The textural properties of the prepared products are studied by N₂ sorption. All of the samples show a nanoporous feature (Figure S1). The Brunauer–Emmett–Teller (BET) surface area of LVO/C/

rGO is measured to be 37.35 m² g⁻¹, and the pore diameter is mainly distributed at ~40 nm (Figure S1d).

Scanning electron microscopy (SEM) and transmission electron microscopy (TEM) images recorded the microstructure information of the products (Figure 3a–e). The obtained LVO/C/rGO composite is composed of deflated balloon-like microspheres with diameters of 1–10 μm (Figure 3a,b). From a typical broken microsphere, a large hollow cavity can be observed at the center; the thickness of the microsphere is approximately 0.15 μm. According to previous studies, the hollow cavity is induced by fast solvent evaporation during spray drying, whereas the deflated balloon-like morphology is probably formed through the collapse of the hollow microspheres.⁴⁶ TEM images of the LVO/C/rGO composite show that numerous irregular LVO nanoparticles are uniformly anchored on the folded rGO framework (Figure 3c,d). The size of Li₃VO₄ nanoparticles is measured to be approximately 30 nm, agreeing well with the XRD result. The high-resolution TEM (HRTEM) image (Figure 3e) reveals that the LVO nanoparticles are coated with a thin layer (~10 nm) of amorphous carbon, which can inhibit the aggregation of LVO nanoparticles. The lattice fringes of LVO can be evidently observed, and the interplanar spacings are 0.41, 0.37, and 0.39 nm, assigning to the (110), (101), and (011) planes of the orthorhombic β -LVO, respectively. The diffraction rings in selected-area electron diffraction (SAED) pattern of LVO/C/rGO (Figure S2) indicate the polycrystalline feature of Li₃VO₄. The high-angle annular dark field (HAADF) image (Figure 3f) and energy-dispersive X-ray spectroscopy (EDS) mapping images (Figure 3g–i) of LVO/C/rGO show that V, O, and C are homogeneously distributed in the LVO/C/rGO composite. After etching LVO/C/rGO with hydrochloric acid, a continuous C/rGO skeleton is obtained (Figure S3), suggesting that the LVO/C/rGO composite possesses a continuous carbon matrix for electron conduction. From the above characterizations, we can know that the deflated balloon-like LVO/C/rGO microspheres possess a continuous carbon matrix for electron transport and rich free spaces (hollow cavities and nanopores) for volume change accommodation. Such a unique structure is expected to be appealing for tackling the electrical conductivity and volume change issues of Li₃VO₄.

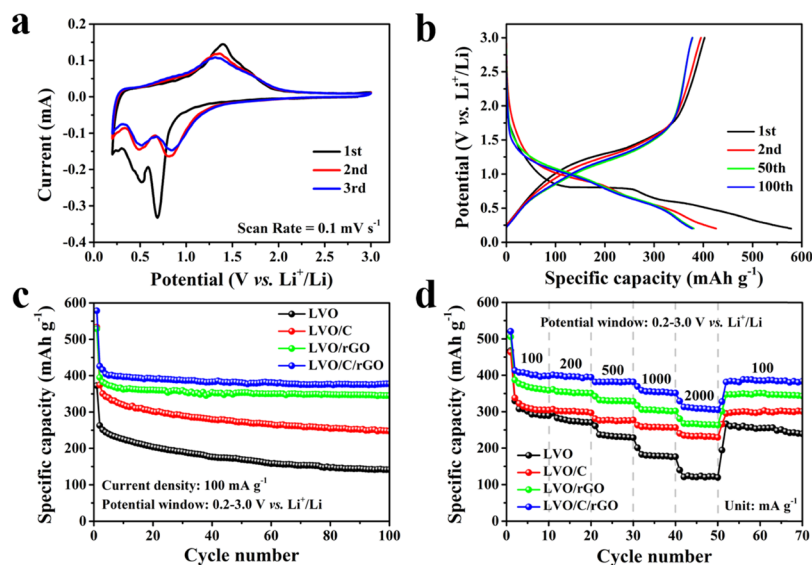


Figure 4. Electrochemical performances in the potential window of 0.2–3.0 V vs Li^+/Li . (a) CV curves of LVO/C/rGO at a scan rate of 0.1 mV s^{-1} ; (b) galvanostatic discharge/charge profiles of LVO/C/rGO at 100 mA g^{-1} ; (c) cycling performances of the samples at a current density of 100 mA g^{-1} ; and (d) rate performances of LVO, LVO/C, LVO/rGO, and LVO/C/rGO.

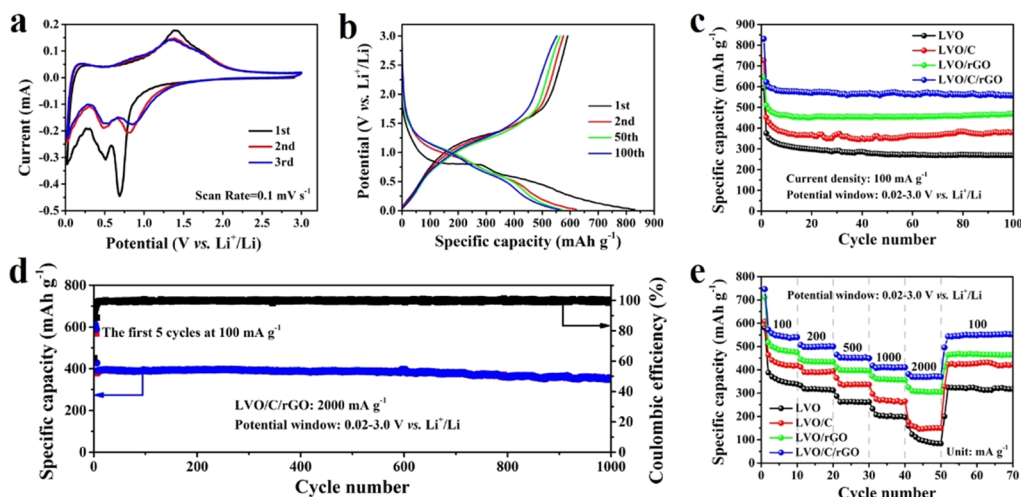


Figure 5. Electrochemical performances of LVO/C/rGO in the potential window of 0.02–3.0 V vs Li^+/Li . (a) CV curves of LVO/C/rGO at a scan rate of 0.1 mV s^{-1} ; (b) galvanostatic discharge/charge profiles of LVO/C/rGO at 100 mA g^{-1} ; (c) cycling performances of the samples at 100 mA g^{-1} ; (d) long-term cycling performance of LVO/C/rGO at 2000 mA g^{-1} ; and (e) rate performances of LVO, LVO/C, LVO/rGO, and LVO/C/rGO.

The morphologies of LVO, LVO/rGO, and LVO/C are shown in Figures S4–S6, respectively. LVO is composed of hollow microspheres with rough nanoparticulate surface (Figure S4). Besides the hollow spheres, nanosheets can also be observed in LVO, which may be caused by the breaking down of hollow microspheres. When GO is employed as the carbon precursor, LVO/rGO microspheres with rough surface are obtained (Figure S5). When PVP is employed as the carbon precursor, LVO/C microspheres with a highly porous foam-like shell and a large hollow cavity at the center (Figure S6) can be obtained. Because of the existence of the hollow cavity, some microspheres collapse, forming a deflated balloon-like morphology similar to that of LVO/C/rGO.

The lithium storage performances of the products are evaluated in half cells. A potential window of 0.2–3.0 V (vs Li^+/Li) for shallow discharging/charging is first employed. Cyclic voltammetry (CV) profiles of LVO/C/rGO are shown

in Figure 4a. Two main reduction peaks at ~ 0.69 and 0.52 V are detected in the cathodic process, which are associated with the reduction of V^{5+} to V^{4+} and V^{4+} to V^{3+} during Li^+ insertion. The peaks shift to 0.83 and 0.50 V in the subsequent cycles. Two evident oxidation peaks at ~ 0.86 and 1.36 V are observed in the anodic processes, corresponding to the oxidation of V^{3+} to V^{4+} and V^{4+} to V^{5+} during Li^+ extraction.

Representative galvanostatic discharge/charge profiles of LVO/C/rGO are shown in Figure 4b. The initial discharge and charge capacities are 578.6 and $402.6 \text{ mA h g}^{-1}$, and the calculated initial Coulombic efficiency (ICE) is 69.6% . The initial irreversible capacity loss is caused by the formation of solid electrolyte interphase film.^{10,47} Although the ICE of LVO/C/rGO is relatively low compared to that of graphite and $\text{Li}_4\text{Ti}_5\text{O}_{12}$, it can be improved by performing prelithiation.⁴⁸ LVO/C/rGO manifests a quite stable capacity of $\sim 400 \text{ mA h g}^{-1}$ at 100 mA g^{-1} (Figure 4c), corresponding to the

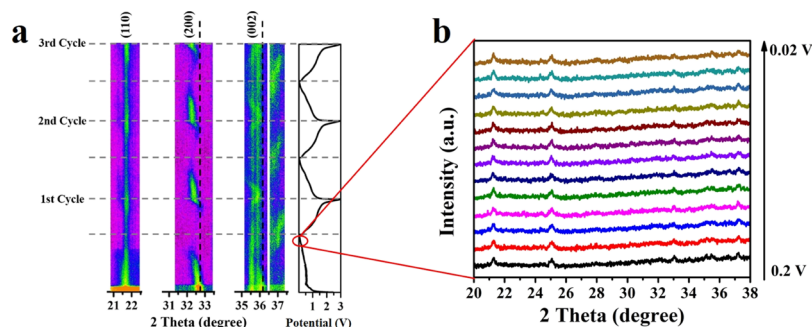


Figure 6. (a) In situ XRD patterns and the corresponding discharge/charge curves of LVO/C/rGO during the first three cycles in the potential window of 0.02–3.0 V at a current density of 200 mA g⁻¹ and (b) in situ XRD patterns of LVO/C/rGO in the selected potential window of 0.02–0.2 V during the initial discharge process.

reversible intercalation/de-intercalation of 2 Li⁺ per formula of Li_{3+x}VO₄. A stable capacity of 378 mA h g⁻¹ can be obtained after 100 cycles, which is superior to that of LVO (103 mA h g⁻¹), LVO/C (248 mA h g⁻¹), and LVO/rGO (345 mA h g⁻¹). The rate performances of the samples are also investigated (Figure 4d). The LVO/C/rGO composite demonstrated the highest discharge capacities at various testing current densities. LVO/C/rGO delivers discharge capacities of 413, 401, 383, 359, and 313 mA h g⁻¹ at current densities of 100, 200, 500, 1000, and 2000 mA g⁻¹, respectively. When the testing current density is returned to 100 mA g⁻¹, a reversible capacity of 389 mA h g⁻¹ can be resumed.

Given the nanoporous feature of LVO/C/rGO is advantageous for volume change accommodation, the lithium storage performances during deep discharging/charging (0.02–3.0 V vs Li⁺/Li) are also investigated. Even under such conditions, LVO/C/rGO shows high lithium intercalation/de-intercalation reversibility, as can be demonstrated from the overlap of the second and third CV profiles (Figure 5a). Galvanostatic discharge/charge profiles of LVO/C/rGO at 100 mA g⁻¹ are exhibited in Figure 5b. Extending the potential window from 0.2–3.0 to 0.02–3.0 V enhances the specific capacity of the sample obviously (Figure S7). With an extended potential window, the initial discharge and charge capacities of LVO/C/rGO in the potential window of 0.02–3.0 V reach 830 and 591 mA h g⁻¹, respectively (Figure 5c). Such a high charge capacity corresponds to the extraction of 3 Li⁺ from per formula of Li_{3+x}VO₄. Interestingly, extending the potential window does not sacrifice the cycling performance. After 100 deep discharge/charge cycles at 100 mA g⁻¹, a capacity of 560 mA h g⁻¹ is retained. Remarkably, the deflated balloon-like morphology remains stable after 100 deep discharge/charge cycles (Figure S8), demonstrating the excellent structural stability of LVO/C/rGO. Compared to LVO/C/rGO, LVO, LVO/C, and LVO/rGO display lower specific capacity. The long-term cyclic property of LVO/C/rGO is evaluated at 2000 mA g⁻¹ (Figure 5d). LVO/C/rGO maintains a stable capacity of 350 mA h g⁻¹ after 1000 cycles, with an outstanding capacity retention of 92.1% (against the sixth cycle). The rate performances of the samples are evaluated by setting the current densities in 100–2000 mA g⁻¹ (Figures 5e and S9). LVO/C/rGO delivers discharge capacities of 572, 507, 465, 418, and 372 mA h g⁻¹ at current densities of 100, 200, 500, 1000, and 2000 mA g⁻¹, respectively. The discharge capacity can be recovered to 554 mA h g⁻¹ when the testing current density resets to 100 mA g⁻¹. Notably, with the gradual

increase of current density from 100 to 2000 mA g⁻¹, no distinct change in discharge/charge profiles can be observed (Figure S9). From the above half-cell measurements, it can be concluded that the “double-carbon”-decorated LVO (LVO/C/rGO) demonstrates better lithium storage performances than bare LVO and “single-carbon”-decorated LVO (LVO/C and LVO/rGO).

To understand the superior electrochemical performances of LVO/C/rGO under deep discharging/charging conditions (0.02–3.0 V), in situ XRD characterization is performed (Figure 6). In general, the main diffraction peaks experience a series of highly reversible changes during cycling, including appearance/disappearance of diffractions, intensity changes, and/or peak shifts. Several obvious changes can be observed during discharging: (I) The (110) diffraction (at ~21.5°) decreases in intensity. (II) The (200) diffraction (at ~32.8°) shifts toward low angles, weakens gradually, and disappears finally. The peak shift suggests a solid-solution reaction mechanism. (III) A new diffraction peak appears at ~37.0° at the late stages of discharge, suggesting a two-phase reaction mechanism. Such changes can be fully reversed during charging. The above results clearly indicate that the lithium storage in Li₃VO₄ is realized through the combination of both solid-solution reaction and two-phase reaction mechanisms. After zooming in at the potential window of 0.02–0.2 V, no distinct change in peak intensity and location can be observed (Figure 6b), suggesting that the intercalation of the third Li⁺ does not induce significant change in the crystal structure of Li_{3+x}VO₄. Considering the in situ XRD results, it is not surprising that LVO/C/rGO manifests outstanding cyclability under both shallow and deep discharging/charging conditions.

Electrochemical impedance spectroscopy (EIS) measurements are used to analyze the charge-transfer process of the samples (Figure S10). Each Nyquist plot is composed of a compressed semicircle and a sloping line. Generally, the depressed semicircle in the high-frequency range describes the charge-transfer resistance (R_{ct}) in the interface of electrolyte/electrode. According to the equivalent circuit (Figure S10), the R_{ct} value of the LVO/C/rGO electrode is 92.5 Ω, which is smaller than that of LVO/rGO (99.5 Ω), LVO/C (104.5 Ω), and LVO (111.0 Ω), indicating that LVO/C/rGO possesses the highest electrical conductivity among the four samples.

To further verify the potential application of LVO/C/rGO, lithium-ion full cells are assembled using commercial LiNi_{0.8}Co_{0.15}Al_{0.05}O₂ as the cathode and LVO/C/rGO as the anode. The full cell is operated at 100 mA g⁻¹ with a voltage range of 1.5–4.0 V, and the capacity is calculated on the basis

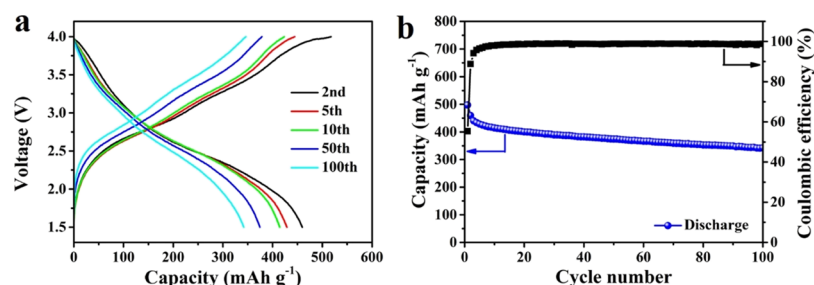


Figure 7. (a) Charge/discharge profiles and (b) cycling performance and the corresponding Coulombic efficiency of the LVO/C/rGO//LiNi_{0.8}Co_{0.15}Al_{0.05}O₂ full cell at 100 mA g⁻¹.

of the loading mass of the LVO/C/rGO electrode. The LVO/C/rGO//LiNi_{0.8}Co_{0.15}Al_{0.05}O₂ full cell shows an operating voltage of ~ 2.8 V (Figure 7a). An impressive capacity of ~ 500 mA h g⁻¹ is obtained initially and then maintaining 346 mA h g⁻¹ after 100 cycles at 100 mA g⁻¹ (Figure 7b).

4. CONCLUSIONS

In summary, deflated balloon-like LVO/C/rGO microspheres with continuous electron transport pathways and sufficient free space for volume change accommodation were prepared through a scalable spray-drying method. The resultant LVO/C/rGO composite demonstrated a high intercalation capacity of 591 mA h g⁻¹ with outstanding cycling stability. A capacity of 560 mA h g⁻¹ can be obtained after 100 cycles at 100 mA g⁻¹, and a stable capacity of 350 mA h g⁻¹ can be achieved after 1000 cycles at 2000 mA g⁻¹ under deep discharging/charging conditions (0.02–3.0 V). The in situ XRD patterns show that lithium is stored through both solid-solution reaction and two-phase reaction mechanisms. The high intercalation capacity and outstanding cyclability make LVO/C/rGO microspheres an appealing anode material for next-generation LIBs.

■ ASSOCIATED CONTENT

Supporting Information

The Supporting Information is available free of charge on the ACS Publications website at DOI: 10.1021/acsami.8b08483.

Materials characterization, electrochemical measurements, and Scherrer equation calculated result; BET results and EIS spectra of all samples; SEM images, TEM images, HAADF images, and EDS mappings of LVO, LVO/C, and LVO/rGO; SAED image, galvanostatic discharge/charge profiles of LVO/C/rGO; and SEM and TEM images of LVO/C/rGO after cycling (PDF)

■ AUTHOR INFORMATION

Corresponding Authors

*E-mail: liangzhou@whut.edu.cn (L.Z.).

*E-mail: mlq518@whut.edu.cn (L.M.).

ORCID

Liang Zhou: 0000-0001-6756-3578

Liqiang Mai: 0000-0003-4259-7725

Notes

The authors declare no competing financial interest.

■ ACKNOWLEDGMENTS

This work was supported by the National Natural Science Fund for Distinguished Young Scholars (51425204), the National Natural Science Foundation of China (51521001, 21673171, and 51502226), the National Key Research and Development Program of China (2016YFA0202603), the Programme of Introducing Talents of Discipline to Universities (B17034), the Yellow Crane Talent (Science & Technology) Program of Wuhan City and the Fundamental Research Funds for the Central Universities (WUT: 2017III009 and 2017III008).

■ REFERENCES

- (1) Tarascon, J.-M.; Armand, M. Issues and Challenges Facing Rechargeable Lithium Batteries. *Nature* **2001**, *414*, 359–367.
- (2) Armand, M.; Tarascon, J.-M. Building Better Batteries. *Nature* **2008**, *451*, 652–657.
- (3) Manthiram, A. Materials Challenges and Opportunities of Lithium Ion Batteries. *J. Phys. Chem. Lett.* **2011**, *2*, 176–184.
- (4) Noorden, R. V. The Rechargeable Revolution: A Better Battery. *Nature* **2014**, *507*, 26–28.
- (5) Tang, Y.; Zhang, Y.; Li, W.; Ma, B.; Chen, X. Rational Material Design for Ultrafast Rechargeable Lithium-Ion Batteries. *Chem. Soc. Rev.* **2015**, *44*, 5926–5940.
- (6) Etacheri, V.; Marom, R.; Elazari, R.; Salitra, G.; Aurbach, D. Challenges in the Development of Advanced Li-Ion Batteries: a Review. *Energy Environ. Sci.* **2011**, *4*, 3243–3262.
- (7) Tang, Y.; Zhang, Y.; Deng, J.; Wei, J.; Tam, H. L.; Chandran, B. K.; Dong, Z.; Chen, Z.; Chen, X. Mechanical Force-Driven Growth of Elongated Bending TiO₂-based Nanotubular Materials for Ultrafast Rechargeable Lithium Ion Batteries. *Adv. Mater.* **2014**, *26*, 6111–6118.
- (8) Kuwano, J.; West, A. R. New Li⁺ ion conductors in the system, Li₄GeO₄-Li₃VO₄. *Mater. Res. Bull.* **1980**, *15*, 1661–1667.
- (9) Li, H.; Liu, X.; Zhai, T.; Li, D.; Zhou, H. Li₃VO₄: A Promising Insertion Anode Material for Lithium-Ion Batteries. *Adv. Energy Mater.* **2013**, *3*, 428–432.
- (10) Liao, C.; Zhang, Q.; Zhai, T.; Li, H.; Zhou, H. Development and perspective of the insertion anode Li₃VO₄ for lithium-ion batteries. *Energy Storage Mater.* **2017**, *7*, 17–31.
- (11) Ni, S.; Zhang, J.; Ma, J.; Yang, X.; Zhang, L.; Li, X.; Zeng, H. Approaching the Theoretical Capacity of Li₃VO₄ via Electrochemical Reconstruction. *Adv. Mater. Interfaces* **2016**, *3*, 1500340.
- (12) Liang, Z.; Lin, Z.; Zhao, Y.; Dong, Y.; Kuang, Q.; Lin, X.; Liu, X.; Yan, D. New understanding of Li₃VO₄/C as potential anode for Li-ion batteries: Preparation, structure characterization and lithium insertion mechanism. *J. Power Sources* **2015**, *274*, 345–354.
- (13) Arroyo-de Dompablo, M. E.; Tartaj, P.; Amarilla, J. M.; Amador, U. Computational Investigation of Li Insertion in Li₃VO₄. *Chem. Mater.* **2016**, *28*, 5643–5651.
- (14) Shen, L.; Chen, S.; Maier, J.; Yu, Y. Carbon-Coated Li₃VO₄ Spheres as Constituents of an Advanced Anode Material for High-Rate Long-Life Lithium-Ion Batteries. *Adv. Mater.* **2017**, *29*, 1701571.

- (15) Liao, C.; Wen, Y.; Xia, Z.; Qin, R.; Liu, X.; Yu, Y.; Shan, B.; Zhai, T.; Li, H. Si-Doping Mediated Phase Control from β - to γ -Form Li₃VO₄ toward Smoothing Li Insertion/Extraction. *Adv. Energy Mater.* **2018**, *8*, 1701621.
- (16) Shi, Y.; Wang, J.-Z.; Chou, S.-L.; Wexler, D.; Li, H.-J.; Ozawa, K.; Liu, H.-K.; Wu, Y.-P. Hollow Structured Li₃VO₄ Wrapped with Graphene Nanosheets in Situ Prepared by a One-Pot Template-Free Method as an Anode for Lithium-Ion Batteries. *Nano Lett.* **2013**, *13*, 4715–4720.
- (17) Tartaj, P.; Amarilla, J. M.; Vazquez-Santos, M. B. Aerosol-Assisted Synthesis of Colloidal Aggregates with Different Morphology: Toward the Electrochemical Optimization of Li₃VO₄ Battery Anodes Using Scalable Routes. *Chem. Mater.* **2016**, *28*, 986–993.
- (18) Fu, Q.; Du, F.; Bian, X.; Wang, Y.; Yan, X.; Zhang, Y.; Zhu, K.; Chen, G.; Wang, C.; Wei, Y. Electrochemical performance and thermal stability of Li_{1.18}Co_{0.15}Ni_{0.15}Mn_{0.52}O₂ surface coated with the ionic conductor Li₃VO₄. *J. Mater. Chem. A* **2014**, *2*, 7555–7562.
- (19) Zhang, C.; Song, H.; Liu, C.; Liu, Y.; Zhang, C.; Nan, X.; Cao, G. Fast and Reversible Li Ion Insertion in Carbon-Encapsulated Li₃VO₄ as Anode for Lithium-Ion Battery. *Adv. Funct. Mater.* **2015**, *25*, 3497–3504.
- (20) Liang, Z.; Zhao, Y.; Ouyang, L.; Dong, Y.; Kuang, Q.; Lin, X.; Liu, X.; Yan, D. Synthesis of carbon-coated Li₃VO₄ and its high electrochemical performance as anode material for lithium-ion batteries. *J. Power Sources* **2014**, *252*, 244–247.
- (21) Zhang, C.; Liu, C.; Nan, X.; Song, H.; Liu, Y.; Zhang, C.; Cao, G. Hollow-Cuboid Li₃VO₄/C as High-Performance Anodes for Lithium-Ion Batteries. *ACS Appl. Mater. Interfaces* **2016**, *8*, 680–688.
- (22) Yang, Y.; Li, J.; He, X.; Wang, J.; Sun, D.; Zhao, J. A facile spray drying route for mesoporous Li₃VO₄/C hollow spheres as an anode for long life lithium ion batteries. *J. Mater. Chem. A* **2016**, *4*, 7165–7168.
- (23) Lim, E.; Lim, W.-G.; Jo, C.; Chun, J.; Kim, M.-H.; Roh, K. C.; Lee, J. Rational design of Li₃VO₄@carbon core-shell nanoparticles as Li-ion hybrid supercapacitor anode materials. *J. Mater. Chem. A* **2017**, *5*, 20969–20977.
- (24) Qin, R.; Shao, G.; Hou, J.; Zheng, Z.; Zhai, T.; Li, H. One-pot synthesis of Li₃VO₄@C nanofibers by electrospinning with enhanced electrochemical performance for lithium-ion batteries. *Sci. Bull.* **2017**, *62*, 1081–1088.
- (25) Shao, G.; Gan, L.; Ma, Y.; Li, H.; Zhai, T. Enhancing the performance of Li₃VO₄ by combining nanotechnology and surface carbon coating for lithium ion batteries. *J. Mater. Chem. A* **2015**, *3*, 11253–11260.
- (26) Zhao, D.; Cao, M. Constructing Highly Graphitized Carbon-Wrapped Li₃VO₄ Nanoparticles with Hierarchically Porous Structure as a Long Life and High Capacity Anode for Lithium-Ion Batteries. *ACS Appl. Mater. Interfaces* **2015**, *7*, 25084–25093.
- (27) Hu, S.; Song, Y.; Yuan, S.; Liu, H.; Xu, Q.; Wang, Y.; Wang, C.-X.; Xia, Y.-Y. A hierarchical structure of carbon-coated Li₃VO₄ nanoparticles embedded in expanded graphite for high performance lithium ion battery. *J. Power Sources* **2016**, *303*, 333–339.
- (28) Li, Q.; Wei, Q.; Sheng, J.; Yan, M.; Zhou, L.; Luo, W.; Sun, R.; Mai, L. Mesoporous Li₃VO₄/C Submicron-Ellipsoids Supported on Reduced Graphene Oxide as Practical Anode for High-Power Lithium-Ion Batteries. *Adv. Sci.* **2015**, *2*, 1500284.
- (29) Jian, Z.; Zheng, M.; Liang, Y.; Zhang, X.; Gheyhani, S.; Lan, Y.; Shi, Y.; Yao, Y. Li₃VO₄ anchored graphene nanosheets for long-life and high-rate lithium-ion batteries. *Chem. Commun.* **2015**, *51*, 229–231.
- (30) Jin, X.; Lei, B.; Wang, J.; Chen, Z.; Xie, K.; Wu, F.; Song, Y.; Sun, D.; Fang, F. Pomegranate-like Li₃VO₄/3D graphene networks nanocomposite as lithium ion battery anode with long cycle life and high-rate capability. *J. Alloys Compd.* **2016**, *686*, 227–234.
- (31) Liu, J.; Lu, P.-J.; Liang, S.; Liu, J.; Wang, W.; Lei, M.; Tang, S.; Yang, Q. Ultrathin Li₃VO₄ nanoribbon/graphene sandwich-like nanostructures with ultrahigh lithium ion storage properties. *Nano Energy* **2015**, *12*, 709–724.
- (32) Yang, Y.; Li, J.; Huang, J.; Huang, J.; Zeng, J.; Zhao, J. Polystyrene-template-assisted synthesis of Li₃VO₄/C/rGO ternary composite with honeycomb-like structure for durable high-rate lithium ion battery anode materials. *Electrochim. Acta* **2017**, *247*, 771–778.
- (33) Ni, S.; Lv, X.; Zhang, J.; Ma, J.; Yang, X.; Zhang, L. The Electrochemical Performance of Lithium Vanadate/Natural Graphite Composite Material as Anode for Lithium Ion Batteries. *Electrochim. Acta* **2014**, *145*, 327–334.
- (34) Li, Q.; Sheng, J.; Wei, Q.; An, Q.; Wei, X.; Zhang, P.; Mai, L. A unique hollow Li₃VO₄/carbon nanotube composite anode for high rate long-life lithium-ion batteries. *Nanoscale* **2014**, *6*, 11072–11077.
- (35) Yang, Y.; Li, J.; Chen, D.; Zhao, J. Spray Drying-Assisted Synthesis of Li₃VO₄/C/CNTs Composites for High-Performance Lithium Ion Battery Anodes. *J. Electrochem. Soc.* **2016**, *164*, A6001–A6006.
- (36) Ni, S.; Lv, X.; Ma, J.; Yang, X.; Zhang, L. The fabrication of Li₃VO₄/Ni composite material and its electrochemical performance as anode for Li-ion battery. *Electrochim. Acta* **2014**, *130*, 800–804.
- (37) Wang, K.; Zhang, C.; Fu, H.; Liu, C.; Li, Z.; Ma, W.; Lu, X.; Cao, G. Enhanced Electrochemical Properties of Li₃VO₄ with Controlled Oxygen Vacancies as Li-Ion Battery Anode. *Chem.—Eur. J.* **2017**, *23*, 5368–5374.
- (38) Zhang, C.; Wang, K.; Liu, C.; Nan, X.; Fu, H.; Ma, W.; Li, Z.; Cao, G. Effects of high surface energy on lithium-ion intercalation properties of Ni-doped Li₃VO₄. *NPG Asia Mater.* **2016**, *8*, No. e287.
- (39) Dong, Y.; Duan, H.; Park, K.-s.; Zhao, Y. Mo⁶⁺ Doping in Li₃VO₄ Anode for Li-Ion Batteries: Significantly Improve the Reversible Capacity and Rate Performance. *ACS Appl. Mater. Interfaces* **2017**, *9*, 27688–27696.
- (40) Zhou, J.; Zhao, B.; Song, J.; Chen, B.; Ma, X.; Dai, J.; Zhu, X.; Sun, Y. Optimization of Rate Capability and Cyclability Performance in Li₃VO₄ Anode Material through Ca Doping. *Chem.—Eur. J.* **2017**, *23*, 16338–16345.
- (41) Wang, K.; Fu, H.; Li, Z.; Xia, M.; Liang, X.; Qi, R.; Cao, G.; Lu, X. Enhancing the Rate Performance of a Li₃VO₄ Anode through Cu Doping. *ChemElectroChem* **2018**, *5*, 478–482.
- (42) Mu, C.; Lei, K.; Li, H.; Li, F.; Chen, J. Enhanced Conductivity and Structure Stability of Ti⁴⁺ Doped Li₃VO₄ as Anodes for Lithium-Ion Batteries. *J. Phys. Chem. C* **2017**, *121*, 26196–26201.
- (43) Shi, Y.; Gao, J.; Abruña, H. D.; Li, H.-J.; Liu, H.-K.; Wexler, D.; Wang, J.-Z.; Wu, Y. The Mechanism of the One-Step Synthesis of Hollow-Structured Li₃VO₄ as an Anode for Lithium-Ion Batteries. *Chem.—Eur. J.* **2014**, *20*, 5608–5612.
- (44) Li, Q.; Wei, Q.; Wang, Q.; Luo, W.; An, Q.; Xu, Y.; Niu, C.; Tang, C.; Mai, L. Self-template synthesis of hollow shell-controlled Li₃VO₄ as a high-performance anode for lithium-ion batteries. *J. Mater. Chem. A* **2015**, *3*, 18839–18842.
- (45) Hummers, W. S., Jr.; Offeman, R. E. Preparation of Graphitic Oxide. *J. Am. Chem. Soc.* **1958**, *80*, 1339.
- (46) Zhu, Y.; Choi, S. H.; Fan, X.; Shin, J.; Ma, Z.; Zachariah, M. R.; Choi, J. W.; Wang, C. Recent Progress on Spray Pyrolysis for High Performance Electrode Materials in Lithium and Sodium Rechargeable Batteries. *Adv. Energy Mater.* **2017**, *7*, 1601578.
- (47) Liao, C.; Wen, Y.; Shan, B.; Zhai, T.; Li, H. Probing the capacity loss of Li₃VO₄ anode upon Li insertion and extraction. *J. Power Sources* **2017**, *348*, 48–56.
- (48) Kim, H. J.; Choi, S.; Lee, S. J.; Seo, M. W.; Lee, J. G.; Deniz, E.; Lee, Y. J.; Kim, E. K.; Choi, J. W. Controlled Prelithiation of Silicon Monoxide for High Performance Lithium-Ion Rechargeable Full Cells. *Nano Lett.* **2016**, *16*, 282–288.